Int. J. Heat Mass Transfer. Vol. 29, No. 1, pp. 59–68, 1986
Printed in Great Britain

0017–9310/86 $3.00 + 0.00
Pergamon Press Ltd.

Some characteristics of longitudinal vortices produced by line-source heating in a low-speed wind tunnel

MAHLON C. SMITH,* DONALD A. HAINES† and WILLIAM A. MAIN†

* Mechanical Engineering Department, Michigan State University, East Lansing, MI 48824 U.S.A.
† North Central Forest Experiment Station, U.S. Department of Agriculture—Forest Service, Stephen S. Nisbet Building, 1407 South Harrison Road, East Lansing, MI 48823, U.S.A.

(*Received* 27 *November* 1984 *and in final form* 15 *July* 1985)

Abstract—Wind tunnel measurements of temperature and velocity fields of a buoyant plume and vortex pair that formed above a heated nichrome wire are described. The differential heating and subsequent temperature gradient, transverse to the main stream flow, produced the longitudinal vortex pair through interaction with the boundary layer. This experiment produced velocity and temperature distributions quite different from those associated with uniform surface heating. The discussion includes possible application to forest fires.

1. INTRODUCTION

LONGITUDINAL vortices may appear in wildland crown-fires where burning is concentrated along the perimeter of the fire. These vortices are of concern in suppression efforts and firefighter safety, particularly as they affect lateral fire spread. They also may be a factor in the formation of unburned tree-crown streets (long strips of scorched but unburned conifer crowns) that are seen in otherwise burned areas following crown fires [1, 2]. These observations prompted the research described herein.

Initial experiments in a wind tunnel showed that when air flowed above and parallel to a heated metal ribbon, simulating the flank of a crown fire, a thin, buoyant plume capped with a vortex pair developed along the length of the ribbon [3]. This vortex pair resembled those observed during an experimental burn involving a large outdoor area filled with oil burners [4]. In that field experiment, the smoke column above the burners bifurcated into two horizontally inclined, counter-rotating vortices. Similar vortex pairs have been observed in smokestack plumes [5].

The present paper describes laminar flow experiments in a low-speed wind tunnel with emphasis on measurements of the temperature and velocity fields of the buoyant plume and vortex pair forming above a heated wire or heated ribbon. The few reliable field observations of longitudinal vortices occurring with large fires indicate that they form at low-to-moderate wind speeds and exist in the atmospheric boundary layer. Preliminary wind tunnel experiments indicate that vortex pairs form and will sometimes persist for significant distances downstream of heating in a turbulent flow. With the assumption of a general similarity between laminar and turbulent vortex pairs, the laboratory results discussed herein appear applicable to wildland crown-fires.

2. EXPERIMENTAL APPARATUS AND DATA PROCESSING

All experiments were conducted in a low-speed wind tunnel. Figure 1 shows three aspects of the tunnel; a soda straw honeycomb entrance with two screens is followed by a settling chamber that, in turn, is followed by a five-to-one, two-dimensional contraction. All heating occurred along the centerline of the floor of the test section. The primary experiment was conducted using a 0.3-mm-diam. nichrome wire, 45.7 cm long, embedded just below the floor surface. Heating began 2 cm downstream of the entrance of the test section. An application of electrical grade ceramic mortar provided insulation as well as surface smoothness.

A traversing mechanism constructed with a vernier scale was used to measure horizontal distance (perpendicular to the tunnel axis) and a screw mechanism raised and lowered the assembly. A telescope mounted on a second vernier scale measured vertical distance.

Most of the data were obtained using a TSI 1054A hot-wire probe mounted on the traversing mechanism. In separate experiments a calibrated wind vane, also mounted on this mechanism, was used to measure the angle of the velocity vector along the tunnel centerline. The vertical velocity component was determined from this measurement and vane calibration.

A 'smoke pot' mounted about 7 cm below the tunnel floor produced smoke for flow visualization. The smoke was generated by heating a nichrome wire that was immersed in a mixture of light oil and oak–pine sawdust. Smoke entered the tunnel through a small hole (approx. 1 mm diameter) just upstream of the heated portion of the floor. The amount of smoke was controlled by varying the pot temperature and the flow rate of fresh air into the smoke pot. An incandescent light illuminated the tunnel for observations and a laser beam was used during photography.

NOMENCLATURE

A	area
Gr	Grashof number, $g\beta\Delta T_m L^3/U_0^2$
g	gravitational acceleration
H	tunnel height, 7.62 cm
L	an effective length measured from the beginning of the boundary layer
R	nominal radius of area, A
Re	Reynolds number, $U_0 L/\nu$
S	perimeter of cirmulation area, A
ds	unit vector tangent to the perimeter of A
T	local air temperature
dT/dz	temperature gradient in the z-direction
T_∞	air temperature at infinity
T_m	maximum tunnel floor temperature
ΔT	temperature difference, $T - T_\infty$
ΔT_m	temperature difference, $T_m - T_\infty$
U_0	free-stream speed
u_t	average component of **V** parallel to **ds**
V	velocity vector
v	vertical velocity component at centerline
W	tunnel width, 25.4 cm
x	downstream distance
y	distance above tunnel floor
z	transverse distance from centerline.

Greek symbols

α	dimensionless induced velocity, u_t/U_0
β	volume coefficient of expansion
γ	dimensionless radius, R/δ
δ	velocity boundary-layer thickness
ν	kinematic viscosity
$\bar{\omega}$	average boundary-layer vorticity
$\bar{\omega}_l$	average longitudinal vorticity.

Calibration equipment consisted of an inclined manometer for hot-wire velocity data and a Keithley Model 170 electronic thermocouple for temperature data. The vane was calibrated directly. The air stream temperature was measured by operating the TSI hot wire in the low overheat mode with output through a Keithley Model 195 multimeter. Figure 2 shows wind vane calibration data. The slope was constant for two data sets, the offset angle being immaterial.

In addition to random errors, several bias errors existed in the temperature data. A radiation error was estimated by view factor analysis for the hot wire in proximity to the hot tunnel floor. The effects of temperature variations of the ambient air during data taking were corrected by periodically re-zeroing the Keithley multimeter. Also, a temperature sensing error by the hot wire occurred with varying positions of the probe and support assembly relative to the hot air stream. This error was minimized by applying a standard correction and maintaining more or less uniform time intervals during horizontal traverses. The three error corrections totalled less than 5% of the measured maximum temperature rise.

In general, the experimental procedure began with an established steady-state air flow and tunnel floor temperature. A downstream cross-section location was selected and the vertical and horizontal positions of the probe were determined by direct measurement.

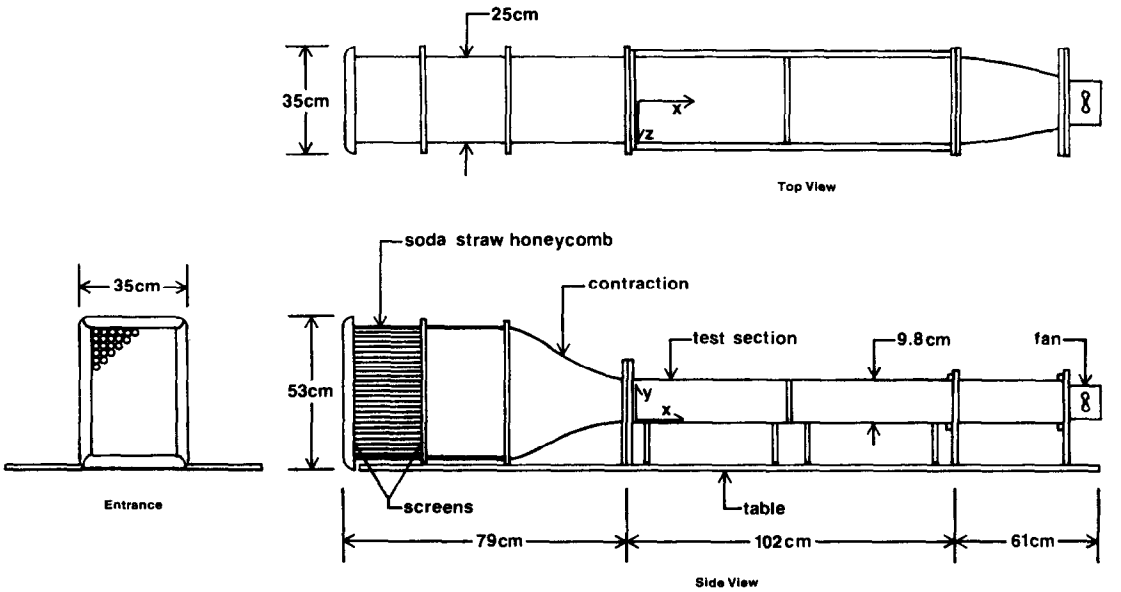

FIG. 1. Entrance, top and side view of the wind tunnel.

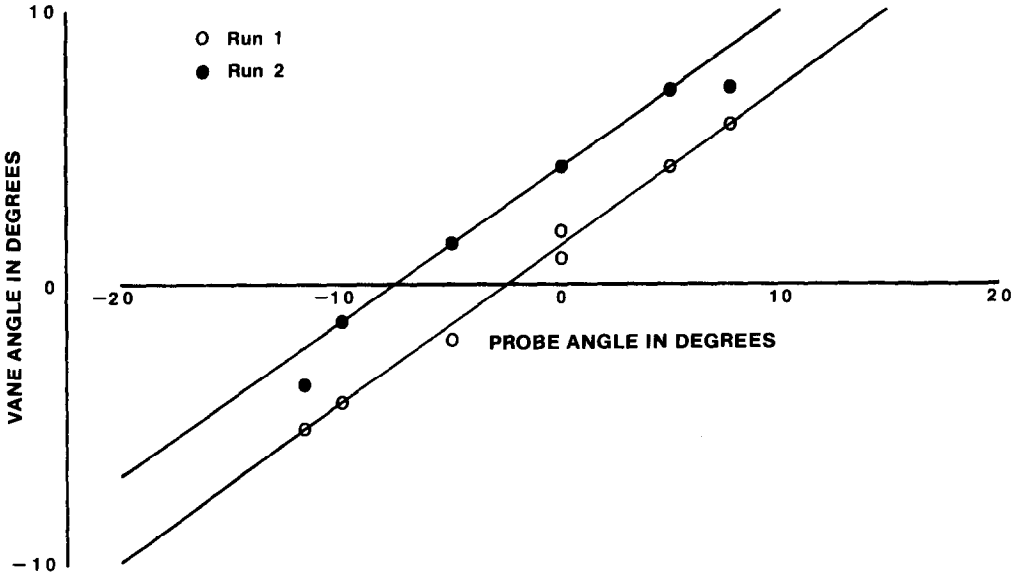

FIG. 2. Calibration results for the wind vane.

Subsequent vernier readings determined the relative probe position. Traverses were made horizontally across the tunnel width for selected vertical positions. The Keithley multimeter provided time-averaged (10 s) data with check runs made periodically. The data shown here are representative rather than averages of many independent runs (e.g. repetitive runs on different days). However, all measurements were taken over several days and appeared to be consistent from cross-section to cross-section. Check runs showed that only small data errors existed.

A computer program was used to correct the temperature measurements for the various error sources at each probe location. The differences between local air temperature and free-stream temperature were made dimensionless by using the maximum tunnel-floor to free-stream temperature difference. The y and z distances were measured from the tunnel floor and centerline, respectively, and scaled as dimensionless values using tunnel height as the scaling parameter.

3. RESULTS AND DISCUSSION

Heat conduction in the tunnel floor caused temperature gradients on the floor surface in contact with the air stream. The downstream gradient $\partial T/\partial x$ was negligible, while Fig. 3 shows the cross-stream gradient, as measured with a thermocouple. The figure

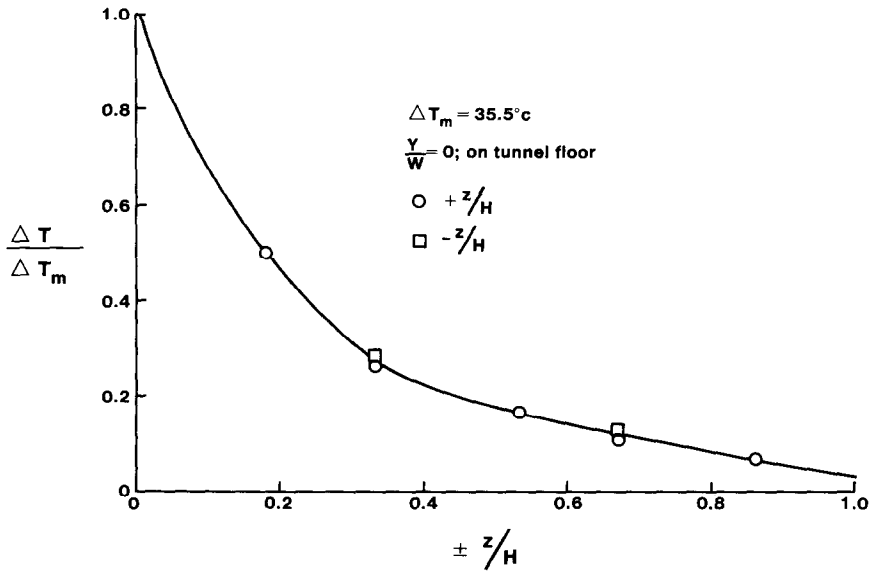

FIG. 3. Temperature distribution from the centerline toward either wall of the tunnel floor.

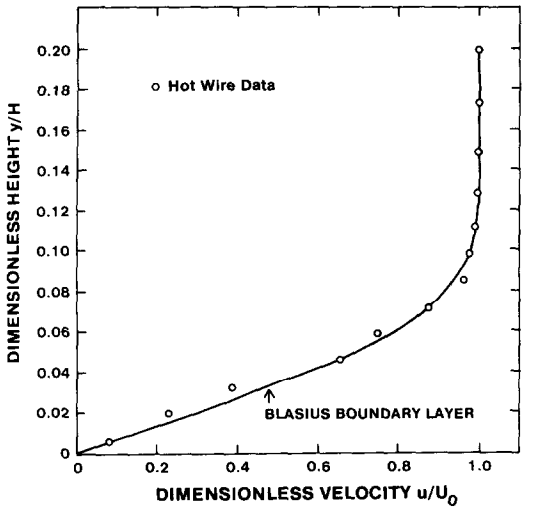

FIG. 4. Downstream velocity profile at the leading edge of the heated region.

shows transverse symmetry about the resistance wire. The total heat transfer rate was 16.5 W. Specific heating was 36.2 W m^{-1} of wire length. The maximum floor temperature was 77.8°C, the maximum air temperature was 35.5°C and the nominal free-stream temperature was 23.3°C. A velocity profile, taken without heating at the beginning of the heating wire, compared well with the Blasius profile (Fig. 4). A constant free-stream speed was maintained during all experiments, 1.1 m s^{-1}, measured at the beginning of heating.

Several temperature traverses were made downstream of the beginning of heating. Figure 5 gives the results of these traverses as isothermal contours. The numbers shown are the temperature rise ratios $\Delta T/\Delta T_m$. Major features include the growth of a central plume of warm air and the subsequent development of two higher temperature lobes on either side of the heating wire.

The downstream vortex development, evident in laser visualization photographs shown in Fig. 6, can be inferred from the temperature contours, considering the paths of fluid elements. Fluid arriving at the vortex core has been swept past the high temperature floor near the centerline. This fluid has contributed to the central warm-air plume at an upstream location. The vorticity has come from the boundary layer where transverse vortex filaments were raised, stretched and rotated to a downstream direction by the buoyant plume. This process has been described previously [3, 4]. The higher diffusion rate of thermal energy as compared with the diffusion of smoke particles has smeared the sharper, streamline smoke pattern.

It is evident that the temperature distributions shown in Fig. 5 are significantly different from those associated with a laminar thermal boundary layer. The horizontal, dashed lines in Fig. 5 give the position of the edge of a normal thermal boundary layer with uniform heating in a laminar flow. The vortices are different also from those described for uniform plate heating [6, 7].

The photographs delineate a number of spatial features. At 17.8 cm downstream from the beginning of

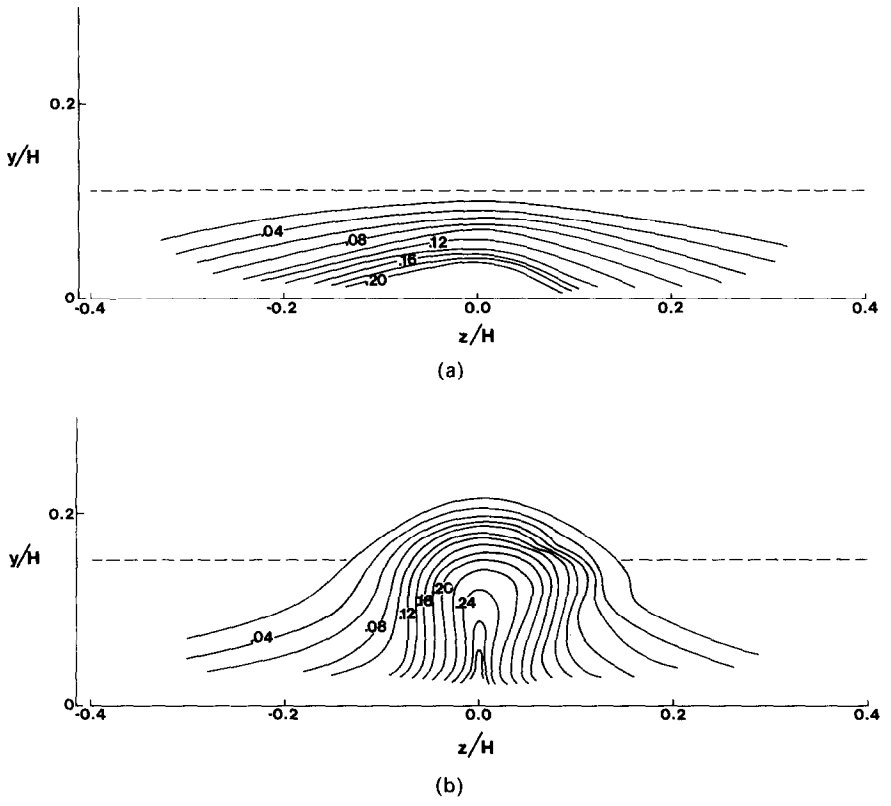

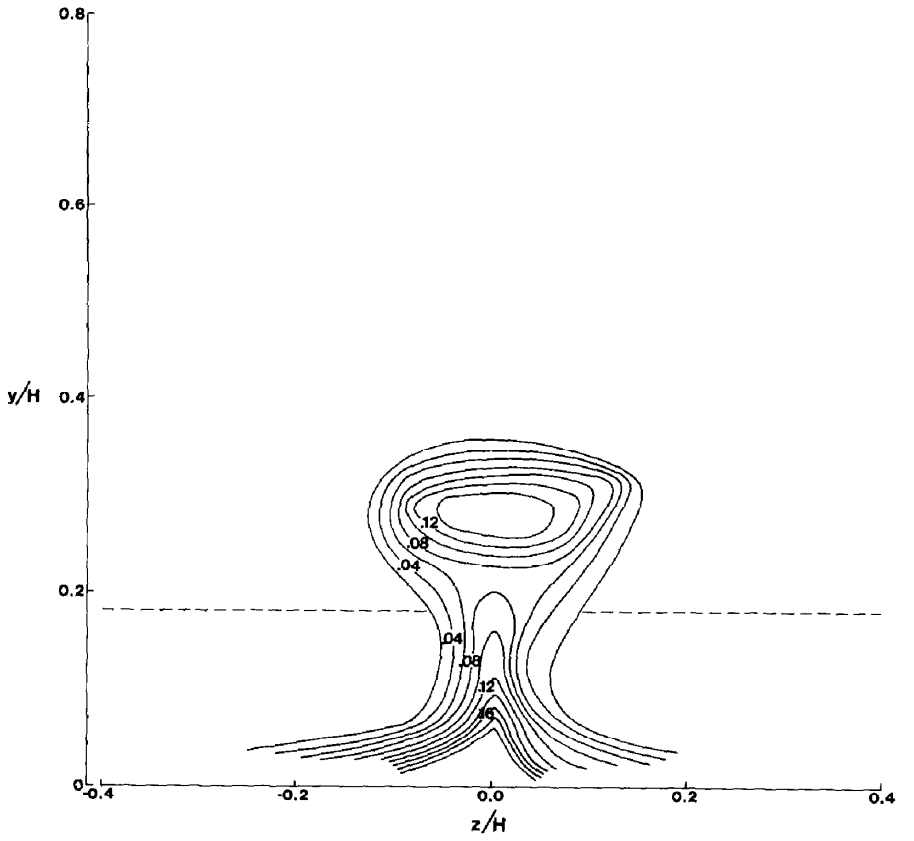

(c)

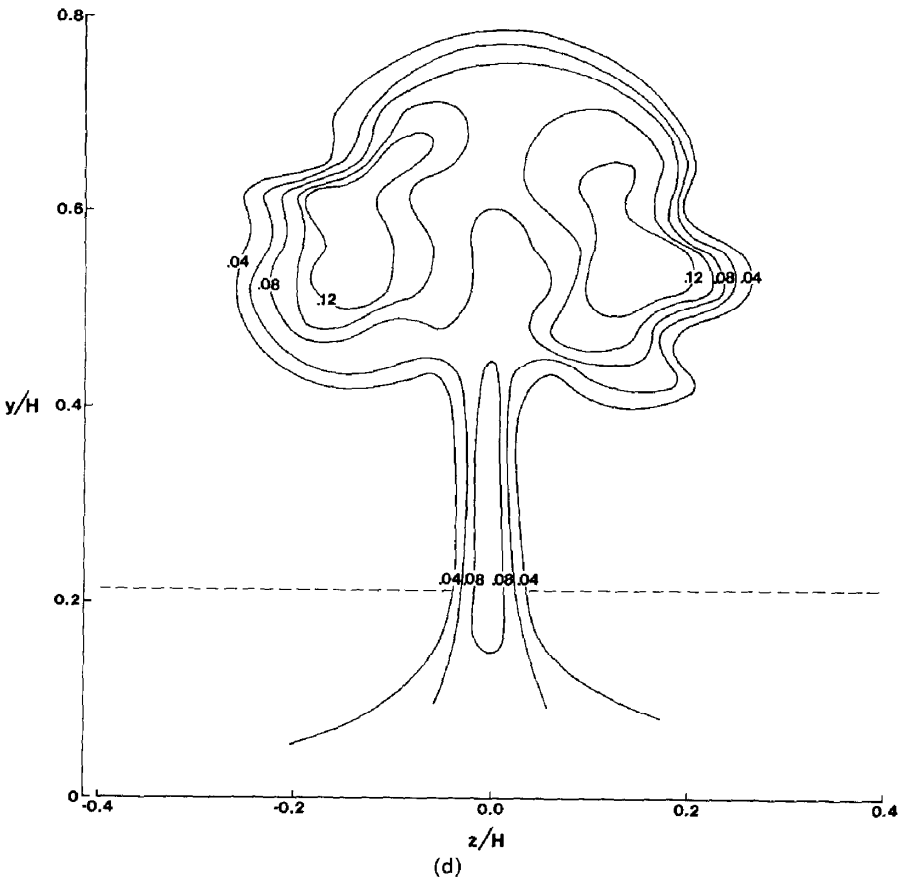

(d)

FIG. 5. Temperature traverses displayed as isothermal contours at the following distances from the beginning of heating: (a) 17.8 cm, (b) 31.4 cm, (c) 45.7 cm, (d) 67.3 cm. Numbers on the contours are $\Delta T/\Delta T_m$. The dashed line indicates the extent of a normal thermal boundary layer.

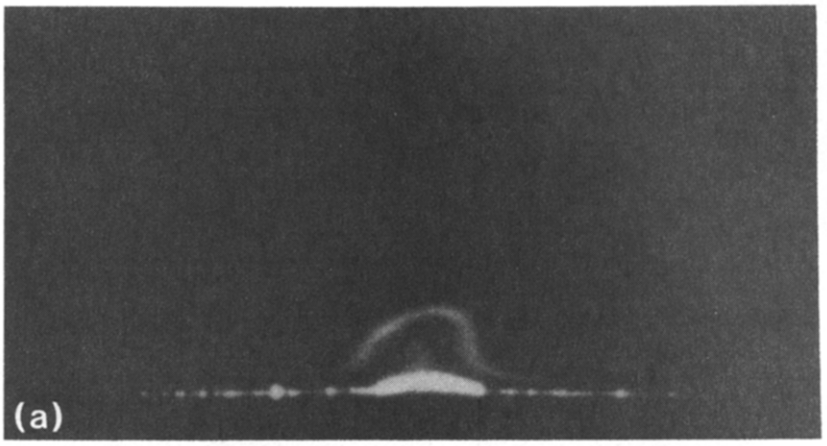

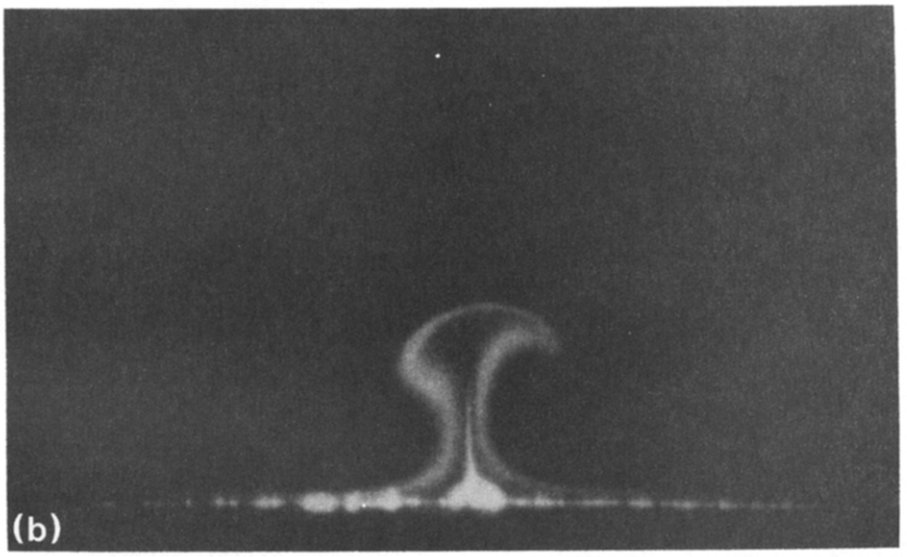

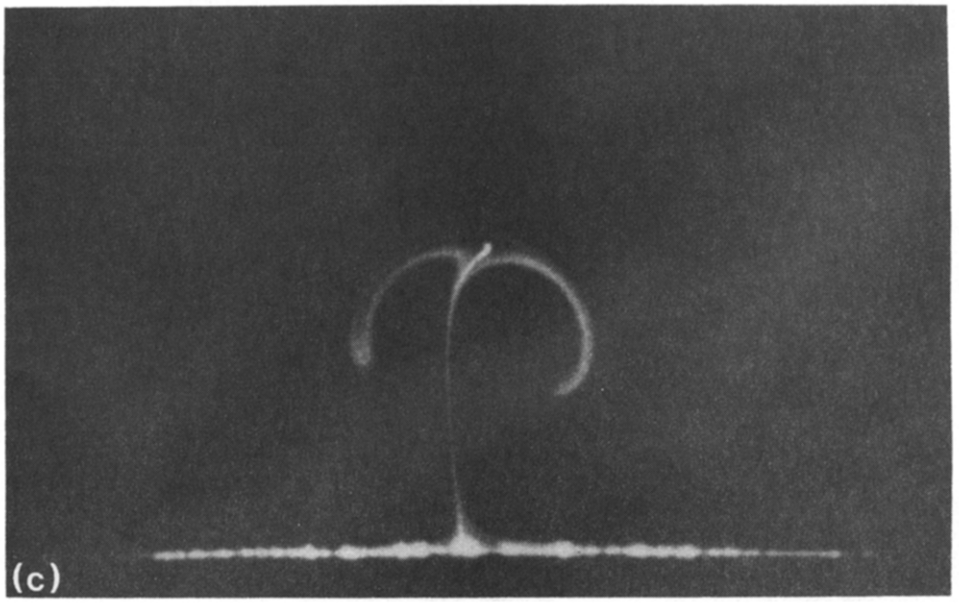

FIG. 6(a)–(c).

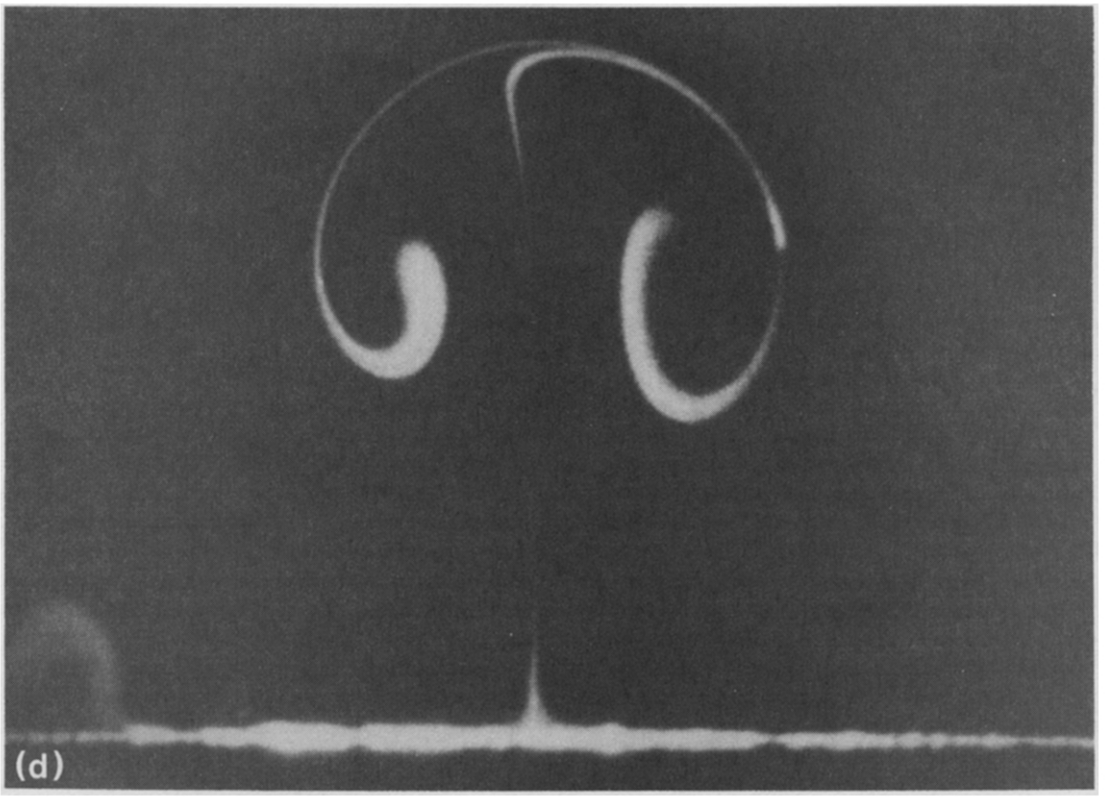

FIG. 6. Laser visualization of the plume and vortex pair over an embedded nichrome wire at the following distances from the beginning of heating: (a) 17.8 cm, (b) 31.4 cm, (c) 45.7 cm, (d) 67.3 cm.

the test section, visualization showed the beginning of the buoyant upwelling [Fig. 6(a)]. A smoke layer capped the warm air that moved away from the heated wire. At 31.4 cm, the somewhat asymmetrical capped layer appeared to be in the initial stages of vortex-pair formation. Heated air flowing upward from the nichrome wire concentrated a spike of smoke that appeared independent of the 'smoke-cap' involved in the initial formation of the downstream vortices [Fig. 6(b)]. At 45.7 cm, the vortex pair was almost fully formed. The photographs do not show clearly the two lines of smoke evident during visual observation, one formed by flow coming into and up the centerline, and the second coming from the 'caps' of the initial buoyant upwelling. Smoke rising along the centerline of the heated wire extended a short distance above the cap in the form of a small spike [Fig. 6(c)]. At 67.3 cm, a distance 6.3 cm downstream of the end of the heated wire, the vortex pair was fully formed [Fig. 6(d)].

Buoyant air near the centerline continued to rise into the fluid structure and was entrained particularly in the right vortex. The smoke images show some asymmetry in the vortex pair. In general, symmetric and asymmetric vortex pairs, with the central stem curving to the right or left, appeared in an apparently random fashion, but were relatively stable when formed. Differences between this vortex pair and those noted previously [6, 7] are due in part to the higher temperature difference, ΔT_m, i.e. about 36°C vs 7°C [6], but result mostly from non-uniform heating.

Wind vane data were obtained by telescope and protractor as vane angle vs vertical position along the centerline of the tunnel at selected downstream distances. This procedure was used because cross-wire measurements were not sufficiently sensitive. The vane angle was used to obtain the vertical velocity component, v, using the calibration data of Fig. 2. Figure 7 shows typical cross-stream data taken at two

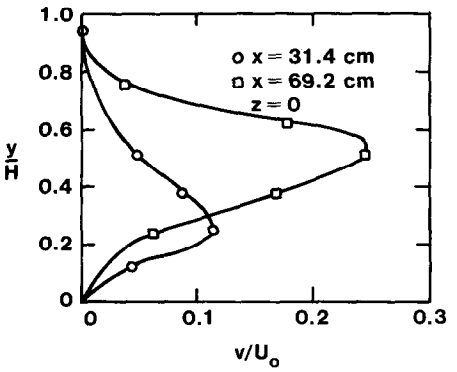

FIG. 7. Vertical velocities at two locations along the tunnel centerline.

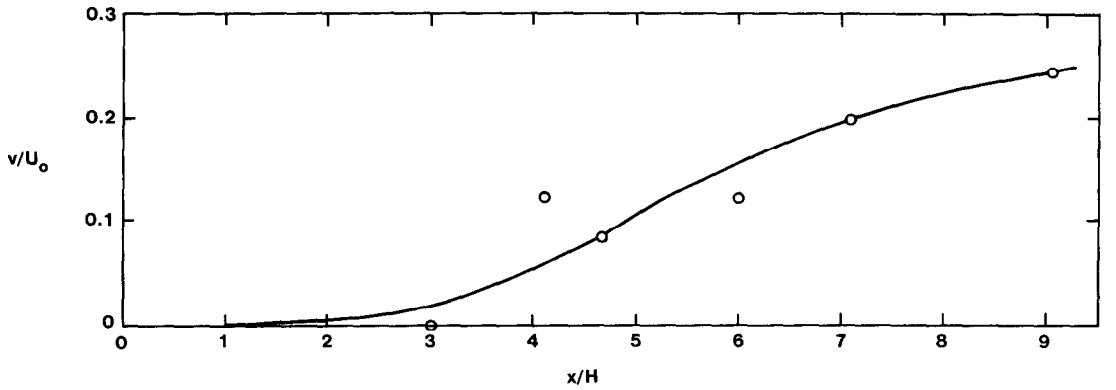

FIG. 8. Crossplot of the location of the maximum value of the vertical velocity along the tunnel centerline.

downstream locations. Figure 8 shows a crossplot of the vertical location of the maximum value of v along the tunnel centerline as a function of downstream position. The vertical velocity component results from both buoyancy effects and induced motion due to the vortices.

The peak vertical velocity components along the centerline occurred at approximately the same height as the vortex cores. The maximum value occurred at the furthest downstream location, 67.3 cm, and was about 25% of the nominal downstream air flow speed. Variations of downstream speed were not large enough to measure. However, it is evident from the inward spiralling vortices that higher downstream speeds must occur near the vortex core to satisfy conservation of mass. The centerline vertical speed increased monotonically with distance downstream, increasing more rapidly initially and less rapidly at locations downstream of the end of heating (Fig. 8).

The vortex pair has three significant dimensions that are especially well defined in the photographs. These are the center plume height, the vortex core height and the core spacing. The thermal plume height is less well defined, although so indicated only indirectly in Fig. 6. The vortex pair grows as it proceeds downstream and thus the significant dimensions increase.

The vortex pair and even the hot air plume were not produced at the leading edge of heating. It takes some time, and thus distance, for the boundary layer to become heated and the buoyant forces to accelerate the flow vertically. This is indicated by the vertical velocity component data shown in Fig. 7 and was observed with smoke visualization. Auxiliary experiments with variations in tunnel speed and heat transfer rate indicated that plume height decreased with speed and increased with heat transfer rate at any given downstream location.

A separate experiment using a single heating wire lying on the surface produced a vortex structure essentially unchanged from Fig. 6. A second separate experiment using a wide (10 cm) heating ribbon produced multiple (three) vortex pairs of approximately the same dimensions. These results suggest that the boundary-layer thickness is the significant length parameter for the core spacing and that the transverse temperature gradient is secondary, although a length dimension can be written as $\Delta T_m/(dT/dz)$.

Typically, the Grashof number and the Reynolds number are the important dimensionless parameters for mixed convection flow. These are generally defined using the streamwise distance, x, as the length parameter. In this instance, due to the low Reynolds number, a significant boundary-layer length existed upstream of the beginning of heating. This length (L) can be estimated (17 cm) using the measured δ (0.8 cm) at the beginning of heating by employing the Blasius boundary-layer approximation. The distance from the beginning of heating to the observed instability producing the vortex pair was about 22 cm. Thus, an approximation to x can be obtained by adding these distances. The Grashof and Reynolds numbers, so calculated, are then 4.8×10^8 and 2.9×10^4, respectively. This point falls approximately on the data correlation curve for Blasius flow instability due to heating from below as given by Gilpin *et al.* [6].

If the boundary-layer thickness at the beginning of heating is the significant length parameter for determining vortex pair dimensions when a velocity boundary layer exists at the initiation of heating, then the downstream growth of the vortex pair will correlate with x/δ. In terms of δ, the average vorticity in the boundary layer can be approximated by

$$\bar{\omega} = \frac{1}{\delta}\int_0^{\delta} \frac{\partial u}{\partial y}\,dy = U_0/\delta. \tag{1}$$

This vorticity contributes to the development of the vortex pair. The definition of vorticity permits a representation of the longitudinal vorticity as

$$\bar{\omega}_1 = \int_S \frac{\mathbf{V}\cdot\mathbf{ds}}{A}. \tag{2}$$

For a circular section this can be written as

$$\bar{\omega}_1 = \frac{2\alpha}{\gamma}\bar{\omega} \tag{3}$$

where $\alpha = |u_i|/U_0$ and $\gamma = R/\delta$, dimensionless-induced velocity and vortex radius, respectively.

The quantity α is analogous to the swirl ratio discussed by investigators of vortices with vertical axes [8, 9]. The present experiments indicate that $|u_t|/U_0$ is about 0.2 at the downstream position, 67.3 cm. A nominal vortex radius, R, as indicated by the smoke photograph in Fig. 6(d), was determined to be about 0.8 cm, the same value as δ at the beginning of heating. For γ of 1.0, equation (3) yields

$$\bar{\omega}_1 = 0.4\bar{\omega}. \quad (4)$$

It is evident that $\bar{\omega}_1$ will decrease downstream as the vortex pair grows. Thus, it appears correct to estimate the longitudinal downstream vorticity as equalling the boundary-layer vorticity near the beginning of heating.

4. CONCLUDING REMARKS

Except for the smoke photographs, there was no documentation of the formation process of the longitudinal vortex pair from the transverse vorticity of the boundary layer. The photographs (Fig. 6) show rising of the flow over the heated portion of the floor, inflow to the centerline, and subsequent downstream vortex flow. The acceleration of the rising hot air plume and subsequent turning and stretching of the vortex lines can be inferred [3], but the effects of boundary-layer velocity profile, heat transfer rate and transverse temperature gradient have not been established.

As indicated by Turner [10] and documented in other observations, in time a laminar vortex pair will dissipate or break down into turbulence. When the boundary layer is already turbulent (as in wildland crown-fires), although vortex pairs form, as has been observed in the field and in our laboratory, it remains to be seen under what specific circumstances this phenomenon will occur. Also, at this time it is not known to what extent the vortices contribute to the production of unburned tree crown streets as discussed by Haines [1]. The present experiments indicate that the formation of downstream vortex pairs occurs in laminar flow heat transfer if the heating produces a significant surface-to-fluid temperature difference and a sufficient transverse temperature gradient. These conditions certainly are satisfied in wildland crown-fires with perimeter burning. Given the visual similarities between the vortices produced during these wind tunnel experiments and those observed during crown-fires, it appears that this laboratory simulation approaches conditions occurring in nature, even though at this point the experiments have not included vortex pairs in turbulent flow.

Acknowledgment—The authors thank James Sumbler, Michigan State University, for the photography.

REFERENCES

1. D. A. Haines, Horizontal roll vortices and crown fires, *J. appl. Met.* **21**, 751–763 (1982).
2. A. J. Simard, D. A. Haines, R. W. Blank and J. S. Frost, The Mack Lake Fire, U.S. Department of Agriculture, Forest Service, North Central Forest Experiment Station, St. Paul, MN, Gen. Tech. Rep. NC-83, pp. 24–28 (1983).
3. D. A. Haines and M. C. Smith, Wind tunnel generation of horizontal roll vortices over a differentially heated surface, *Nature* **306**, 351–352 (1983).
4. C. R. Church, J. T. Snow and J. Dessens, Intense atmospheric vortices associated with a 1000 MW fire, *Bull. Am. met. Soc.* **61**, 682–694 (1980).
5. R. S. Scorer, *Air Pollution*, 1st edn, Chap. 2. Pergamon Press, Oxford (1968).
6. R. R. Gilpin, H. Imura and K. C. Cheng, Experiments on the onset of longitudinal vortices in horizontal Blasius flow heated from below, *J. Heat Transfer* **100**, 71–77 (1978).
7. R. Wu and K. C. Cheng, Thermal instability of Blasius flow along horizontal plates, *Int. J. Heat Mass Transfer* **19**, 907–913 (1976).
8. G. A. Briggs, Plume rise from multiple sources, Cooling Tower Environment-1974, ERDA symposium series, CONF-740302, pp. 161–177 (1974).
9. C. R. Church, J. T. Snow, G. L. Baker and E. Magee, Characteristics of tornado-like vortices as a function of swirl ratio: a laboratory investigation, *J. atmos. Sci.* **36**, 1755–1776 (1979).
10. J. S. Turner, A comparison between buoyant vortex rings and vortex pairs, *J. Fluid Mech.* **7**, 419–433 (1960).

QUELQUES CARACTERISTIQUES DES TOURBILLONS LONGITUDINAUX PRODUITS PAR UN CHAUFFAGE AVEC UNE SOURCE LINEAIRE DANS UNE SOUFFLERIE A FAIBLE VITESSE

Résumé—On décrit des mesures en soufflerie de champs de température et de vitesse d'un panache et d'une paire de tourbillons formés au dessus d'un fil de nichrome chauffé. Le chauffage différentiel et le gradient de température résultant, transverse à l'écoulement moyen principal, produisent la paire de tourbillons longitudinaux par interaction avec la couche limite. Cette expérience produit des distributions de vitesse et de température très différentes de celles associées à un chauffage superficiel uniforme. La discussion inclut une possible application aux feux de forêt.

LÄNGSWIRBEL BEI LINIENFÖRMIGER WÄRMEFREISETZUNG UND GERINGER ÜBERLAGERTER STRÖMUNGSGESCHWINDIGKEIT

Zusammenfassung—Windkanalmessungen des Temperatur- und Geschwindigkeitsfeldes einer Auftriebsfahne und eines Wirbelpaares, die sich über einem beheizten Cr–Ni-Draht bilden, werden beschrieben. Intermittierendes Heizen und die daraus resultierenden Temperaturgradienten quer zur Hauptströmungsrichtung erzeugen das Wirbelpaar durch Wechselwirkung mit der Grenzschicht. Dieses Experiment erzeugte Geschwindigkeits- und Temperaturverteilungen, die sich stark von denen bei einheitlicher Heizung der Oberfläche unterscheiden. Die Diskussion schließt mögliche Anwendungen bei Waldbränden ein.

НЕКОТОРЫЕ ХАРАКТЕРИСТИКИ ПРОДОЛЬНЫХ ВИХРЕЙ, ГЕНЕРИРУЕМЫХ ЛИНЕЙНЫМ ИСТОЧНИКОМ ТЕПЛА В НИЗКОСКОРОСТНОЙ АЭРОДИНАМИЧЕСКОЙ ТРУБЕ

Аннотация—Описаны измерения в аэродинамической трубе полей температур и скорости свободновосходящей струи, а также процесс слияния вихрей, образующихся над нагреваемой нихромовой проволокой. Пара продольных вихрей образовывалась в результате ступенчатого нагрева проволоки и возникающего температурного градиента, направленного поперек набегающего потока. Полученные в таком эксперименте распределения скоростей и температур полностью отличаются от полей при равномерном нагреве поверхности. Рассматривается возможность применения результатов к решению проблемы лесных пожаров.